

Nonlinear Control of a Planar Magnetic Levitation System

Michel Lévis

Dept. of Electrical and Computer Engineering
University of Toronto
Toronto, 10 King's College Circle M5S3G4
levis@control.utoronto.ca

Manfredi Maggiore

Dept. of Electrical and Computer Engineering
University of Toronto
Toronto, 10 King's College Circle M5S3G4
maggiore@control.utoronto.ca

Abstract— In this paper, we derive the model of a three-magnet positioning device and design a nonlinear control that stabilizes it. The motivation of this work is to develop tools that may have practical significance to, e.g., photolithography and to create a challenging nonlinear control problem which can be used to test novel nonlinear control approaches. The nonlinear controller designed here transforms the nonlinear system with three positive inputs into a linear system in controllable canonical form with two inputs. A simple linear controller (e.g., an LQR controller) can then be designed to stabilize the system. Finally, the nonlinear controller is robustified to handle uncertainties that affect planar levitation devices.

I. INTRODUCTION

Figure 1 demonstrates a plan view of the system and the forces exerted on the disk by each magnet. Each of the rectangles represents an electromagnet with a ferromagnetic core with N coil windings. The circle in the middle of the plane is a disk, also of ferromagnetic material. Although not shown in the diagram, the actual system has another magnet suspended above the three magnets shown. The additional magnet producing a force in the z direction is independent of the magnets in the xy plane. That is, the system is comprised of two decoupled subsystems - the base magnets formed in a triangle and the suspended magnet above this plane. The discussion will focus on the coupled, nonlinear xy subsystem at the base.

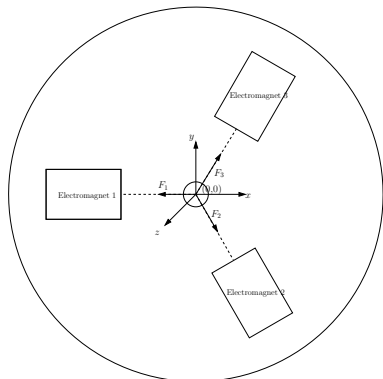


Fig. 1. Forces acting on disk when at origin.

Although magnetic levitation positioning devices have been investigated in the past (see, e.g. [6] and [3]), none of them include the triangular arrangement shown in Figure 1 which has the advantage of minimizing the number of electromagnets needed to actuate two degrees of freedom. Furthermore, the controller stabilizing similar systems (see, e.g., [6], where linear motors are used) is often constructed from the linearized system. That is, the system is linearized about a certain operating point and then, using common linear control techniques, the system is stabilized. This paper initiates a research which aims to develop a rigorous nonlinear control framework to solve the set point regulation problem for such systems, and leads to some interesting problems which will be the object of future investigation.

The first section develops the basic electromagnetic analysis needed to derive the dynamics of the disk from a single magnet. This one-dimensional result is then expanded in the xy plane to find the equations of the forces acting on the disk from all three magnets, which we use to find the state-space representation of the disk's dynamics. The second section discusses the nonlinear control design of the system. This discussion is divided into two parts. In the first part we derive a feedback transformation yielding linear dynamics and use it to design a controller solving the problem. Then, in the second part, Lyapunov redesign is performed to compensate for uncertainties. In the third section of the paper, we compare the performance of our nonlinear controller and a controller developed from the linearized system. The last section will finalize the results and discuss future prospects of the research.

II. MODELLING

The equations describing the motion of the disk are

$$\ddot{x} = \frac{F_x(x, y, I_1, I_2, I_3)}{m} \quad (1)$$

$$\ddot{y} = \frac{F_y(x, y, I_1, I_2, I_3)}{m}. \quad (2)$$

The forces F_x and F_y are generated by the electromagnets in the x and y direction, respectively. In this section we develop a mathematical model of the system depicted in Figure 1 using superposition of the forces and neglecting the fringing effect of the magnetic flux lines.

The dynamics of the disk can be modelled in four steps

1. Derive the dynamics of the forces acting on the disk from a single electromagnet.
2. Using the result in step 1, perform vector analysis to construct the dynamics of the disk from all three electromagnets.
3. Use the result from step 2 in the motion equations (1) and (2).
4. Find state-space representation.

A. Force Dynamics of Disk from Single Electromagnet

This analysis is standard and the result can be found, e.g. in [7]. The forces are calculated by taking the gradient of the system's magnetic energy. Magnetic energy can be calculated from the magnetic flux. Thus, the first step is to find the magnetic flux through the electromagnets' core. Magnetic flux is found using Ampere's Law [1]

$$\oint_C \vec{H} \cdot d\vec{l} = NI, \quad (3)$$

where N is the number of coil windings and I is the current going through the coils.

Magnetic field lines, \vec{H} , and magnetic flux density lines, \vec{B} , have the following linear relationship when the core is not saturated,

$$\vec{H} = \frac{1}{\mu} \vec{B}. \quad (4)$$

where μ is the core's permeability. Assuming magnetic flux density is constant, the magnetic flux can be calculated in terms of the magnetic flux density and cross sectional area of the core

$$\Phi = BA, \quad (5)$$

where A denotes the area of the cross section for the material. The magnetic flux density near the electromagnet is $\vec{B} = Ba_z$, where a_z is the vector depicted in Figure 2. The magnetic fluxes in the core, Φ_1 , and in the air gap, Φ_2 , are given by

$$\Phi_1 = BA_1 := \Phi \quad (6)$$

$$\Phi_2 = BA_1 = \Phi. \quad (7)$$

The magnetic flux in the disk is expressed in terms of the flux in the core

$$\Phi_3 = BA_2 = \frac{A_2}{A_1} \Phi. \quad (8)$$

Taking the closed path shown in Figure 2, Ampere's Law is used with the necessary substitutions from equations (4), (6), (7) and (8) to get magnetic flux. Thus

$$\begin{aligned} \oint_C \vec{H} \cdot d\vec{l} &= \oint_C \frac{1}{\mu} \vec{B} \cdot d\vec{l} \\ &= \oint_{C_1} \frac{1}{\mu_1} \vec{B} \cdot d\vec{l} + \oint_{C_2} \frac{1}{\mu_o} \vec{B} \cdot d\vec{l} + \oint_{C_3} \frac{1}{\mu_2} \vec{B} \cdot d\vec{l} + 0 \\ &\quad + \oint_{C_5} \frac{1}{\mu_o} \vec{0} \cdot d\vec{l} + 0 \\ &= \frac{L_1}{\mu_1} \frac{\Phi}{A_1} + \frac{z}{\mu_o} \frac{\Phi}{A_1} + \frac{1}{\mu_2} \int_0^{L_2} \frac{\Phi_3}{A_2} dl \\ &= \frac{L_1}{\mu_1 A_1} \Phi + \frac{z}{\mu_o A_1} \Phi + \frac{1}{\mu_2} \int_0^{L_2} \frac{1}{A_2} \frac{A_2}{A_1} \Phi dl \\ &= \left(\frac{L_1}{\mu_1 A_1} + \frac{L_2}{\mu_2 A_1} + \frac{z}{\mu_o A_1} \right) \Phi \\ &= NI. \end{aligned}$$

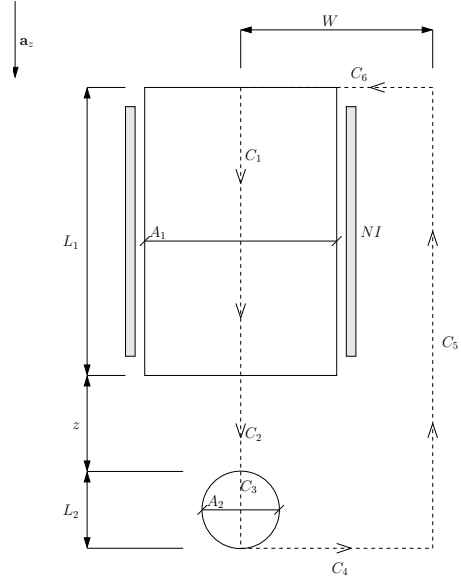


Fig. 2. Amperian path.

The line integrals corresponding to C_4 and C_6 are zero because \vec{B} is perpendicular to the lines C_4 and C_6 . The line integral corresponding to C_5 can be assumed zero by assuming that the lengths of C_4 and C_6 stretch to infinity. Thus, the magnetic flux reads as

$$\Phi = \frac{NI}{\frac{L_1}{\mu_1 A_1} + \frac{L_2}{\mu_2 A_1} + \frac{z}{\mu_o A_1}}. \quad (9)$$

Magnetic energy is defined as

$$W_m = \frac{1}{2} \int_V \vec{B} \cdot \vec{H} dv, \quad (10)$$

where V is the volume of the object subject to \vec{B} and \vec{H} .

Using equations (4), (6), (7), (8), (9) and (10), an expression for the magnetic energy of the system can be given as

$$\begin{aligned} W_m &= \frac{1}{2} \int_V \vec{B} \cdot \vec{H} dv \\ &= \frac{1}{2} \int_V \frac{1}{\mu} B^2 dv \\ &= \frac{1}{2} \left[\int_{V_1} \frac{1}{\mu_1} \left(\frac{\Phi}{A_1} \right)^2 dv + \int_{V_2} \frac{1}{\mu_o} \left(\frac{\Phi}{A_1} \right)^2 dv \right. \\ &\quad \left. + \int_{V_3} \frac{1}{\mu_2} \left(\frac{\Phi_3}{A_2} \right)^2 dv \right] \\ &= \frac{1}{2} \left[\frac{L_1 A_1}{\mu_1 A_1^2} \Phi^2 + \frac{z A_1}{\mu_o A_1^2} \Phi^2 + \int_{V_3} \frac{1}{\mu_2} \left(\frac{1}{A_2} \frac{A_2}{A_1} \Phi \right)^2 dv \right] \\ &= \frac{(NI)^2}{2} \frac{\frac{L_1}{\mu_1 A_1} + \frac{L_2}{\mu_2 A_1} + \frac{z}{\mu_o A_1}}{\left(\frac{L_1}{\mu_1 A_1} + \frac{L_2}{\mu_2 A_1} + \frac{z}{\mu_o A_1} \right)^2}, \end{aligned}$$

where B denotes the magnitude of \vec{B} , h is the height of the disk and $A_r = \frac{4A_1^2}{\pi h L_2}$.

Using the constant current method (see, e.g. [1]), the force is calculated by taking the gradient of the magnetic energy

$$\vec{F}_m = \nabla W_m. \quad (11)$$

Relationship (11) holds true under the assumption that the current is constant. While the current in the system under consideration is not constant, its time variation is typically slow and thus (11) is reasonably accurate (this approximation is common in the literature (see, e.g [7])).

Using equation (11) the force acting on the disk by one electromagnet is

$$\begin{aligned}\vec{F}_m &= \nabla W_m \\ &= \frac{\partial W_m}{\partial z} \mathbf{a}_z \\ &= -\frac{(NI)^2 \frac{L_1}{\mu_1 A_1} - \frac{L_2}{\mu_2 A_1} + \frac{2L_2}{\mu_2 A_r} + \frac{z}{\mu_o A_1}}{2\mu_o A_1 \left(\frac{L_1}{\mu_1 A_1} + \frac{L_2}{\mu_2 A_1} + \frac{z}{\mu_o A_1} \right)^3} \mathbf{a}_z.\end{aligned}$$

Similarly to the standard result, the one-dimensional force expression is proportional to the current squared and to the reciprocal of the distance squared.

B. Vector Analysis and System Dynamics

Using superposition and the results of the previous section, we next derive the forces acting on the disk from all three magnets. The force model of the system is as follows

$$\vec{F}_x = (F_1 \cos \theta_1 + F_2 \cos \theta_2 + F_3 \cos \theta_3) \quad (12)$$

$$\vec{F}_y = (F_1 \sin \theta_1 + F_2 \sin \theta_2 + F_3 \sin \theta_3). \quad (13)$$

Figure 3 shows the angles $\theta_1, \theta_2, \theta_3$ and the forces acting on the disk when it is at a location (x, y) inside the triangle $\triangle P_1 P_2 P_3$, which is assumed to be equilateral. The attractive force from electromagnet i , where $i = 1, 2, 3$, has the expression

$$\vec{F}_i = -\frac{(NI_i)^2 \frac{L_1}{\mu_1 A_1} - \frac{L_2}{\mu_2 A_1} + \frac{2L_2}{\mu_2 A_r} + \frac{z_i}{\mu_o A_1}}{2\mu_o A_1 \left(\frac{L_1}{\mu_1 A_1} + \frac{L_2}{\mu_2 A_1} + \frac{z_i}{\mu_o A_1} \right)^3} \mathbf{a}_{z_i} \quad (14)$$

The value z_i , depicted in Figure 3, is the distance between the center of the disk and the middle point, denoted P_i , of the face of electromagnet i . The distance between the origin and the face of each magnet is d .

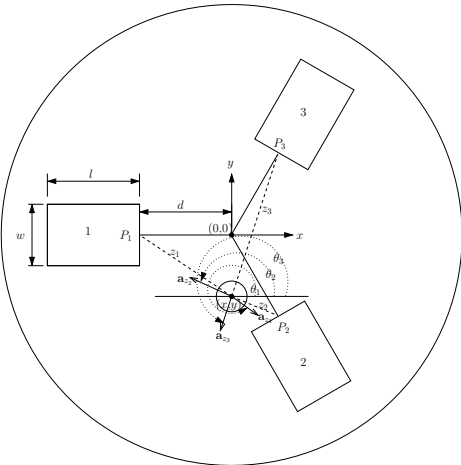


Fig. 3. Distances from center of disk to each magnet.

By expressing the variable distances, z_i , and the trigonometric functions in terms of x and y , equations (12) and (13) can be represented by the disk coordinates and various constants. The state-space representation of the system motion dynamics can now be found. Define the state of the system as

$$\mathbf{x} = \begin{bmatrix} x_1 \\ x_2 \\ x_3 \\ x_4 \end{bmatrix} := \begin{bmatrix} x \\ \dot{x} \\ y \\ \dot{y} \end{bmatrix}. \quad (15)$$

Using this definition and substituting the force expressions into motion equations (1) and (2) gives the dynamics of the entire system

$$\begin{aligned}\dot{x}_1 &= x_2 \\ \dot{x}_2 &= -\frac{1}{2m\mu_o A_1} \left[\varphi_1(x_1, x_3) \cdot (x_1 + d) I_1^2 \right. \\ &\quad \left. + \varphi_2(x_1, x_3) \cdot \left(x_1 - \frac{d}{2} \right) I_2^2 + \varphi_3(x_1, x_3) \cdot \left(x_1 - \frac{d}{2} \right) I_3^2 \right] \\ \dot{x}_3 &= x_4 \\ \dot{x}_4 &= -\frac{1}{2m\mu_o A_1} \left[\varphi_1(x_1, x_3) \cdot (-x_3) I_1^2 \right. \\ &\quad \left. + \varphi_2(x_1, x_3) \cdot \left(x_3 + \frac{\sqrt{3}}{2} d \right) I_2^2 + \varphi_3(x_1, x_3) \cdot \left(x_3 - \frac{\sqrt{3}}{2} d \right) I_3^2 \right] \quad (16)\end{aligned}$$

where

$$\begin{aligned}\varphi_1(x_1, x_3) &= N^2 \frac{\frac{L_1}{\mu_1 A_1} - \frac{L_2}{\mu_2 A_1} + \frac{2L_2}{\mu_2 A_r} + \frac{\sqrt{(x_1+d)^2 + x_3^2}}{\mu_o A_1}}{\left(\frac{L_1}{\mu_1 A_1} + \frac{L_2}{\mu_2 A_1} + \frac{\sqrt{(x_1+d)^2 + x_3^2}}{\mu_o A_1} \right)^3} \\ &\quad \frac{1}{\sqrt{(x_1+d)^2 + x_3^2}} \\ \varphi_2(x_1, x_3) &= N^2 \frac{\frac{L_1}{\mu_1 A_1} - \frac{L_2}{\mu_2 A_1} + \frac{2L_2}{\mu_2 A_r} + \frac{\sqrt{\left(x_1 - \frac{d}{2}\right)^2 + \left(x_3 + \frac{\sqrt{3}}{2} d\right)^2}}{\mu_o A_1}}{\left(\frac{L_1}{\mu_1 A_1} + \frac{L_2}{\mu_2 A_1} + \frac{\sqrt{\left(x_1 - \frac{d}{2}\right)^2 + \left(x_3 + \frac{\sqrt{3}}{2} d\right)^2}}{\mu_o A_1} \right)^3} \\ &\quad \frac{1}{\sqrt{\left(x_1 - \frac{d}{2}\right)^2 + \left(x_3 + \frac{\sqrt{3}}{2} d\right)^2}} \\ \varphi_3(x_1, x_3) &= N^2 \frac{\frac{L_1}{\mu_1 A_1} - \frac{L_2}{\mu_2 A_1} + \frac{2L_2}{\mu_2 A_r} + \frac{\sqrt{\left(x_1 - \frac{d}{2}\right)^2 + \left(x_3 - \frac{\sqrt{3}}{2} d\right)^2}}{\mu_o A_1}}{\left(\frac{L_1}{\mu_1 A_1} + \frac{L_2}{\mu_2 A_1} + \frac{\sqrt{\left(x_1 - \frac{d}{2}\right)^2 + \left(x_3 - \frac{\sqrt{3}}{2} d\right)^2}}{\mu_o A_1} \right)^3} \\ &\quad \frac{1}{\sqrt{\left(x_1 - \frac{d}{2}\right)^2 + \left(x_3 - \frac{\sqrt{3}}{2} d\right)^2}}\end{aligned}$$

Table I lists values of various physical constants in the system used for simulations and other analysis.

III. NONLINEAR CONTROL DESIGN

This section demonstrates the design of two nonlinear controllers - an ideal controller that stabilizes the nominal system and a robust controller that stabilizes

| Parameter | Value |
|-----------|--------------------------------|
| μ_0 | $4\pi \times 10^{-7}$ |
| μ_r | 700 |
| μ_1 | $2.8\pi \times 10^{-4}$ |
| μ_2 | $2.8\pi \times 10^{-4}$ |
| L_1 | 0.1000 m |
| L_2 | 0.0167 m |
| d | 0.0500 m |
| m | 0.5000 kg |
| h | 0.0083 m |
| N | 100 |
| A_1 | 0.01 m^2 |
| A_r | $\frac{2.88}{\pi} \text{ m}^2$ |

TABLE I
VALUES OF PHYSICAL PARAMETERS.

the system affected by uncertainties. Uncertainties are represented in the system as follows

$$\dot{x}_2 = \frac{F_x(x_1, x_3)}{m} + \frac{\delta_1(\mathbf{x})}{m} \quad (17)$$

$$\dot{x}_3 = \frac{F_y(x_1, x_3)}{m} + \frac{\delta_2(\mathbf{x})}{m}. \quad (18)$$

where $\delta_1(\mathbf{x})$ and $\delta_2(\mathbf{x})$ represent unknown forces that have not been taken into account in the modelling.

A. Ideal Control Design

In this section, the design of a nonlinear controller that provides exponential convergence to an equilibrium point is described. The ideal controller does not take uncertainties into account, thus $\delta_1 = 0$ and $\delta_2 = 0$. More precisely, the goal is finding currents I_1 , I_2 and I_3 yielding

$$\begin{aligned} \dot{x}_1 &= x_2 \\ \dot{x}_2 &= z_1 \\ \dot{x}_3 &= x_4 \\ \dot{x}_4 &= z_2, \end{aligned} \quad (19)$$

where z_1 and z_2 are degrees of freedom of the controller. In other words we seek to find a feedback transformation converting (at least on a suitable compact set) the dynamics (16) into a linear system where a well known linear control technique can be applied to stabilize the entire system. Because the control enters the system squared, the main difficulty in the design is finding positive functions for I_i whose combination results in (19).

To this end, we generalize the idea presented in [5], Section 12.3. Attaining $\dot{x}_2 = z_1$ and $\dot{x}_4 = z_2$ can only be achieved by converting (19) to the following problem¹

$$\dot{x}_2 - \dot{x}_4 = z_1 - z_2 \quad (20)$$

$$\dot{x}_2 = z_1 \quad (21)$$

The control design can be broken down into three steps

¹Otherwise, as pointed out in the following, sign indefinite terms arise that prevent positive currents from being found to control the system.

1. Finding smooth positive functions for I_1^2 , I_2^2 and I_3^2 that satisfy equation (20).
2. Substitute I_1^2 , I_2^2 and I_3^2 found in step 1 into (21) and use the available degrees of freedom to satisfy equation (21).
3. Using LQR, design a gain matrix that renders the closed-loop system stable.

In the first part, smooth functions must be found to make $\dot{x}_2 - \dot{x}_4$ become $z_1 - z_2$. The three currents must cooperate together to supply a function that satisfies (20). Similarly to what is done in [5], Section 12.3, we use the following expressions for the currents

$$I_1^2 = \frac{-2m\mu_0 A_1}{\varphi_1 \cdot (x_1 + x_3 + d)} \eta_1 \quad (22)$$

$$I_2^2 = \frac{-2m\mu_0 A_1}{\varphi_2 \cdot \left(x_1 - x_3 - \frac{\sqrt{3}+1}{2}d\right)} \eta_2 \quad (23)$$

$$I_3^2 = \frac{-2m\mu_0 A_1}{\varphi_3 \cdot \left(x_1 - x_3 + \frac{\sqrt{3}-1}{2}d\right)} \eta_3, \quad (24)$$

where η_1 , η_2 and η_3 are degrees of freedom to be defined later. Substituting the currents (22), (23) and (24) into $\dot{x}_2 - \dot{x}_4$ gives

$$\begin{aligned} \dot{x}_2 - \dot{x}_4 &= -\frac{1}{2m\mu_0 A_1} \left[\varphi_1 \cdot (x_1 + x_3 + d) I_1^2 \right. \\ &\quad + \varphi_2 \cdot \left(x_1 - x_3 - \frac{\sqrt{3}+1}{2}d\right) I_2^2 \\ &\quad \left. + \varphi_3 \cdot \left(x_1 - x_3 + \frac{\sqrt{3}-1}{2}d\right) I_3^2 \right] \\ &= -\frac{1}{2m\mu_0 A_1} \left[\varphi_1 \cdot (x_1 + x_3 + d) \frac{-2m\mu_0 A_1}{\varphi_1 \cdot (x_1 + x_3 + d)} \eta_1 \right. \\ &\quad + \varphi_2 \cdot \left(x_1 - x_3 - \frac{\sqrt{3}+1}{2}d\right) \frac{-2m\mu_0 A_1}{\varphi_2 \cdot \left(x_1 - x_3 - \frac{\sqrt{3}+1}{2}d\right)} \eta_2 \\ &\quad \left. + \varphi_3 \cdot \left(x_1 - x_3 + \frac{\sqrt{3}-1}{2}d\right) \frac{-2m\mu_0 A_1}{\varphi_3 \cdot \left(x_1 - x_3 + \frac{\sqrt{3}-1}{2}d\right)} \eta_3 \right] \\ &= \eta_1 + \eta_2 + \eta_3. \end{aligned} \quad (25)$$

The signs of the functions η_1 , η_2 and η_3 must be such that I_1^2 , I_2^2 and I_3^2 are all positive. The function φ_i appearing in I_i is positive, for $i = 1, \dots, 3$, while the constant $-2m\mu_0 A_1$ is negative. The denominators $x_1 + x_3 + d$ and $x_1 - x_3 + \frac{\sqrt{3}-1}{2}d$ in (22) and (24) are positive over the set

$$\mathbf{C} = \left\{ \mathbf{x} \in \mathbb{R}^4 \mid |x_1| \leq \frac{d}{6} \text{ and } |x_3| \leq \frac{d}{6} \right\} \quad (26)$$

The expression $x_1 - x_3 - \frac{\sqrt{3}+1}{2}d$ in the denominator of I_2 is always negative within \mathbf{C} . Thus, in order to guarantee the currents are always positive, the signs of η_1 , η_2 and η_3 must be as follows

$$\eta_1 \leq 0, \eta_2 \geq 0 \text{ and } \eta_3 \leq 0. \quad (27)$$

The actual functions are now to be defined. These functions must be smooth, obey the sign constraints given in

(27) and, according to (25), the sum $\eta_1 + \eta_2 + \eta_3$ must equal $z_1 - z_2$. The following functions satisfy the criteria

$$\eta_1 = \frac{z_1 - z_2 - \sqrt{(z_1 - z_2)^2 + \epsilon}}{4} - A \quad (28)$$

$$\eta_2 = \frac{z_1 - z_2 + \sqrt{(z_1 - z_2)^2 + \epsilon}}{2} + A + B \quad (29)$$

$$\eta_3 = \frac{z_1 - z_2 - \sqrt{(z_1 - z_2)^2 + \epsilon}}{4} - B, \quad (30)$$

where A and B are positive functions that can be freely chosen and are used in the next part of the control design and $\epsilon > 0$. The first step of the design is now complete, in that equation (20) has been satisfied. The second part of the control design involves substituting the currents and choosing A and B such that the second equality (21) can be met. Substituting I_1 , I_2 and I_3 into \dot{x}_2 gives

$$\begin{aligned} \dot{x}_2 &= -\frac{1}{2m\mu_0 A_1} \left[\varphi_1 \cdot (x_1 + d) \frac{-2m\mu_0 A_1}{\varphi_1 \cdot (x_1 + x_3 + d)} \eta_1 \right. \\ &+ \varphi_2 \cdot \left(x_1 - \frac{d}{2} \right) \frac{-2m\mu_0 A_1}{\varphi_2 \cdot \left(x_1 - x_3 - \frac{\sqrt{3}+1}{2}d \right)} \eta_2 \\ &+ \left. \varphi_3 \cdot \left(x_1 - \frac{d}{2} \right) \frac{-2m\mu_0 A_1}{\varphi_3 \cdot \left(x_1 - x_3 + \frac{\sqrt{3}-1}{2}d \right)} \eta_3 \right] \\ &= \frac{x_1 + d}{x_1 + x_3 + d} \left(\frac{z_1 - z_2 - \sqrt{(z_1 - z_2)^2 + \epsilon}}{4} - A \right) \\ &+ \frac{x_1 - \frac{d}{2}}{x_1 - x_3 - \frac{\sqrt{3}+1}{2}d} \left(\frac{z_1 - z_2 + \sqrt{(z_1 - z_2)^2 + \epsilon}}{2} + A + B \right) \\ &+ \frac{x_1 - \frac{d}{2}}{x_1 - x_3 + \frac{\sqrt{3}-1}{2}d} \left(\frac{z_1 - z_2 - \sqrt{(z_1 - z_2)^2 + \epsilon}}{4} - B \right) \\ &= \frac{z_1 - z_2 - \sqrt{(z_1 - z_2)^2 + \epsilon}}{4} \left(\frac{x_1 + d}{x_1 + x_3 + d} \right) \\ &+ \frac{z_1 - z_2 - \sqrt{(z_1 - z_2)^2 + \epsilon}}{4} \left(\frac{x_1 - \frac{d}{2}}{x_1 - x_3 + \frac{\sqrt{3}-1}{2}d} \right) \\ &+ \frac{z_1 - z_2 + \sqrt{(z_1 - z_2)^2 + \epsilon}}{2} \left(\frac{x_1 - \frac{d}{2}}{x_1 - x_3 - \frac{\sqrt{3}+1}{2}d} \right) \\ &+ \left(\frac{x_1 - \frac{d}{2}}{x_1 - x_3 - \frac{\sqrt{3}+1}{2}d} - \frac{x_1 + d}{x_1 + x_3 + d} \right) A \\ &+ \left(\frac{x_1 - \frac{d}{2}}{x_1 - x_3 - \frac{\sqrt{3}+1}{2}d} - \frac{x_1 - \frac{d}{2}}{x_1 - x_3 + \frac{\sqrt{3}-1}{2}d} \right) B. \end{aligned}$$

Define

$$\begin{aligned} f_{\text{neg}} &= \frac{z_1 - z_2 - \sqrt{(z_1 - z_2)^2 + \epsilon}}{4} \left(\frac{x_1 + d}{x_1 + x_3 + d} \right) \\ f_{\text{pos}} &= \frac{z_1 - z_2 - \sqrt{(z_1 - z_2)^2 + \epsilon}}{4} \left(\frac{x_1 - \frac{d}{2}}{x_1 - x_3 + \frac{\sqrt{3}-1}{2}d} \right) \\ &+ \frac{z_1 - z_2 + \sqrt{(z_1 - z_2)^2 + \epsilon}}{2} \left(\frac{x_1 - \frac{d}{2}}{x_1 - x_3 - \frac{\sqrt{3}+1}{2}d} \right) \\ f_a &= \frac{x_1 - \frac{d}{2}}{x_1 - x_3 - \frac{\sqrt{3}+1}{2}d} - \frac{x_1 + d}{x_1 + x_3 + d} \\ f_b &= \frac{x_1 - \frac{d}{2}}{x_1 - x_3 - \frac{\sqrt{3}+1}{2}d} - \frac{x_1 - \frac{d}{2}}{x_1 - x_3 + \frac{\sqrt{3}-1}{2}d}. \end{aligned}$$

Assuming state x is within the set C defined in (26), f_{neg} , f_{pos} , f_a and f_b enjoy the properties

$$\begin{aligned} f_{\text{neg}} &\leq 0 \\ f_{\text{pos}} &\geq 0 \\ f_a &\leq 0 \\ f_b &\geq 0. \end{aligned}$$

Rewrite (31) in terms of the defined functions

$$\dot{x}_2 = f_{\text{neg}} + f_{\text{pos}} + f_a A + f_b B,$$

and notice that, since both A and B must be positive, A can only be used to cancel a positive term while B can only be used to cancel a negative term.

The identity $\dot{x}_2 = z_1$ can now be obtained by choosing A and B as

$$\begin{aligned} A &= -\frac{1}{f_a} \left(f_{\text{pos}} + \frac{-z_1 + \sqrt{z_1^2 + \epsilon}}{2} \right) \\ B &= -\frac{1}{f_b} \left(f_{\text{neg}} + \frac{-z_1 - \sqrt{z_1^2 + \epsilon}}{2} \right). \end{aligned}$$

Remark: If the system of equations had not been solved by finding currents that satisfied $\dot{x}_2 - \dot{x}_4 = z_1 - z_2$ in the first part, then either f_a or f_b would be sign indefinite. This would prevent using a degree of freedom, either A or B , and as a result equation (21) would not be satisfied because the remaining degree of freedom can only cancel one of the two sign definite terms, f_{pos} or

f_{neg} . The first two parts of the nonlinear control are complete: the original system (16) has been transformed into the linear system (19) by means of the following feedback transformation

$$I_1^2 = \frac{-2m\mu_0 A_1}{\varphi_1(x_1 + x_3 + d)} \left(\frac{z_1 - z_2 - \sqrt{(z_1 - z_2)^2 + \epsilon}}{4} - A \right) \quad (32)$$

$$I_2^2 = \frac{-2m\mu_0 A_1}{\varphi_2 \left(x_1 - x_3 - \frac{\sqrt{3}+1}{2}d \right)} \left(\frac{z_1 - z_2 + \sqrt{(z_1 - z_2)^2 + \epsilon}}{2} + A + B \right) \quad (33)$$

$$I_3^2 = \frac{-2m\mu_0 A_1}{\varphi_3 \left(x_1 - x_3 + \frac{\sqrt{3}-1}{2}d \right)} \left(\frac{z_1 - z_2 - \sqrt{(z_1 - z_2)^2 + \epsilon}}{4} - B \right) \quad (34)$$

Notice that, while the original system (16) has three control inputs, (19) has two control inputs, z_1 and z_2 . System (19) can be represented as

$$\dot{x} = \begin{bmatrix} 0 & 1 & 0 & 0 \\ 0 & 0 & 0 & 0 \\ 0 & 0 & 0 & 1 \\ 0 & 0 & 0 & 0 \end{bmatrix} x + \begin{bmatrix} 0 & 0 \\ 1 & 0 \\ 0 & 0 \\ 0 & 1 \end{bmatrix} u \quad (35)$$

where $u = [u_1, u_2]^T$, which is in Brunovsky normal form.

Using LQR, we now design a controller $u = -Kx$ that stabilizes the origin. With the weighing matrices

$$Q = \begin{bmatrix} 5000 & 0 & 0 & 0 \\ 0 & 100 & 0 & 0 \\ 0 & 0 & 700 & 0 \\ 0 & 0 & 0 & 2000 \end{bmatrix}, \quad R = \begin{bmatrix} 5000 & 1000 \\ 1000 & 5000 \end{bmatrix} \quad (36)$$

the following Riccati equation solution, \mathbf{P} , and gain matrix, \mathbf{K} , were generated

$$\mathbf{P} = \begin{bmatrix} 7065.5 & 4955.6 & 137.7 & 340.1 \\ 4955.6 & 7051.7 & 248.6 & 847.8 \\ 137.7 & 248.6 & 2002.6 & 1866.5 \\ 340.1 & 847.8 & 1866.5 & 5349.2 \end{bmatrix},$$

$$\mathbf{K} = \begin{bmatrix} 1.0183 & 1.4338 & -0.0260 & -0.0463 \\ -0.1356 & -0.1172 & 0.3785 & 1.0791 \end{bmatrix}. \quad (37)$$

Assuming no uncertainties, the design for a nonlinear controller that stabilizes the system about an equilibrium point is complete. Notice that tracking can also be straightforwardly achieved for system (19). Controller performance for this specific application is measured in two ways, namely the amplitude of the control input (ie. currents) and the size of the domain of attraction. The goal is to have small currents and a large domain of attraction. The motivation of having low currents is to prevent any of the cores from saturating and to avoid the insulator coating on the electromagnet wire from melting. Through simulation, it was found that most currents do not exceed 5 A although for some initial conditions, the currents peaked to almost 10 A. It is not known exactly at what current the cores will saturate or at what current the magnet coils overheat, however, the aim is to have the control inputs below 6 A.

For the second performance criterion, an estimate of the domain of attraction can be obtained by finding the largest level set of V that fits inside the set \mathcal{C} defined in (26), where our controller is guaranteed to be valid. In other words we want to find the largest value of $c > 0$ such that

$$\Omega_{\mathcal{C}} := \left\{ \mathbf{x} \in \mathbb{R}^4 \mid \mathbf{x}^T \mathbf{P} \mathbf{x} \leq c \right\} \subset \mathcal{C}. \quad (38)$$

This can be done numerically using a constrained optimization technique. By doing that, using the plant parameters in Table I, the estimate of the domain of attraction is

$$\Omega_{\mathcal{C}} = \left\{ \mathbf{x} \in \mathbb{R}^4 \mid V(\mathbf{x}) \leq 0.0938 \right\}. \quad (39)$$

To assess whether $\Omega_{\mathcal{C}}$ is an accurate estimate of the basin of attraction, it would be valuable to visualize it graphically. Figure 4 is a slice of the domain of attraction estimate when the velocities x_2 and x_4 are set to zero. That is, Figure 4 is the level set plot of $\{\mathbf{x} \in \mathbb{R}^4 \mid V(x_1, 0, x_3, 0) \leq 0.0938\}$.

The domain estimate represents the set of feasible locations where the disk can be initialized at zero velocity and driven to the origin. This concludes the design of the ideal nonlinear controller. Simulation results of the system's response using this controller are shown in Section IV.

B. Robust Control Design

In this section, uncertainties δ_1 and δ_2 are taken into account. Uncertainties are compensated for by re-designing the Lyapunov function according to standard Lyapunov redesign (see, e.g, [2]). This technique can only be applied when the matching condition is satisfied, that is when the uncertainties enter the system

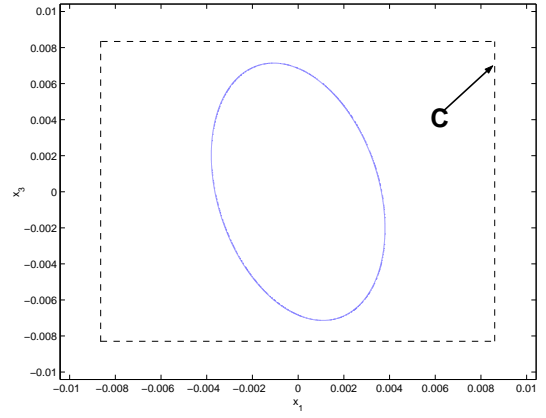


Fig. 4. Domain of attraction estimate.

dynamics at the same point as the control variable. After applying the nonlinear control (32), (33) and (34) to system (17) and (18), we get

$$\dot{\mathbf{x}} = \begin{bmatrix} 0 & 1 & 0 & 0 \\ 0 & 0 & 0 & 0 \\ 0 & 0 & 0 & 1 \\ 0 & 0 & 0 & 0 \end{bmatrix} \mathbf{x} + \begin{bmatrix} 0 & 0 \\ 1 & 0 \\ 0 & 0 \\ 0 & 1 \end{bmatrix} (\mathbf{u} + \delta) \quad (40)$$

where $\mathbf{u} = [z_1, z_2]^T$ and $\delta(\mathbf{x}) = [\delta_1(x_1, x_2, x_3), \delta_2(x_1, x_3, x_4)]^T$, and thus the matching condition is satisfied.

In the previous section, an LQR controller $\mathbf{u} = -\mathbf{K}\mathbf{x} := \Psi(\mathbf{x})$ was designed to stabilize the nominal system (35). Assume that with $\mathbf{u} = \Psi(\mathbf{x}) + \mathbf{v}$ an upper bound, $\rho(\mathbf{x})$, to the uncertain terms exists such that $\|\delta(\mathbf{x})\| \leq \rho(\mathbf{x})$. The upper bound can be found by making a conservative estimate on the uncertainties that may be involved in the system

$$\delta_1(x_1, x_2, x_3) \leq a|x_1| + b|x_3| - kx_2 = \Delta(x_1, x_3) - kx_2 \quad (41)$$

$$\delta_2(x_1, x_3, x_4) \leq \Delta(x_1, x_3) - kx_4 \quad (42)$$

where $a, b \in \mathbb{R}$, $\Delta(x_1, x_3) := a|x_1| + b|x_3|$ and $k \in \mathbb{R}^+$ is the unknown coefficient of friction.

The $\Delta(x_1, x_3)$ term in δ_1 and δ_2 is an unknown force that represents the inaccuracy of our model if the disk does not remain within the region where superposition holds or if the assumption that the attractive forces acting on the disk point towards the center of each magnets' face does not hold. Also, because friction was not included in the modelling, the last term in the uncertainties δ_1 and δ_2 include a Coulomb friction expression.

Realistic bounds can be placed on these uncertainties, $|a|, |b| \leq \beta_1$ and $k \leq \beta_2$, where $\beta_1, \beta_2 \in \mathbb{R}^+$. Using these restrictions, the upper bound to $\|\delta(\mathbf{x})\|$ is

$$\begin{aligned} \|\delta(\mathbf{x})\|_2 &= \sqrt{|\delta_1|^2 + |\delta_2|^2} \\ &\leq \left[2\beta_1^2 (|x_1| + |x_3|)^2 + 2\beta_2^2 (|x_1| + |x_3|)(|x_2| + |x_4|) \right. \\ &\quad \left. + x_2^2 + x_4^2 \right]^{\frac{1}{2}} \\ &:= \rho(\mathbf{x}) \end{aligned}$$

where $\beta^* = \max\{\beta_1, \beta_2\}$.

The additional control term, \mathbf{v} , is added to $\Psi(\mathbf{x})$ so that $\mathbf{u} = \Psi(\mathbf{x}) + \mathbf{v}$ stabilizes the system with uncertainties (40). Apply $\mathbf{u} = \Psi(\mathbf{x}) + \mathbf{v}$ to (40) and perform Lyapunov analysis

$$\begin{aligned}\dot{V} &= \mathbf{x}^T \mathbf{P}\dot{\mathbf{x}} + \dot{\mathbf{x}}^T \mathbf{P}\mathbf{x} \\ &= -\mathbf{x}^T \mathbf{Q}\mathbf{x} + 2\mathbf{x}^T \mathbf{P}\mathbf{B}(\mathbf{v} + \delta(\mathbf{x})) \\ &\leq -\lambda_{\min}(\mathbf{Q})\|\mathbf{x}\|_2^2 + \omega^T(\mathbf{v} + \delta(\mathbf{x})) \\ &\leq -\lambda_{\min}(\mathbf{Q})\|\mathbf{x}\|_2^2 + \omega^T \mathbf{v} + \|\omega\|_2 \|\delta\|_2 \\ &\leq -\lambda_{\min}(\mathbf{Q})\|\mathbf{x}\|_2^2 + \omega^T \mathbf{v} + \|\omega\|_2 \rho(\mathbf{x})\end{aligned}$$

where $\lambda_{\min}(\mathbf{Q})$ denotes the minimum eigenvalue of matrix \mathbf{Q} , $\omega^T = 2\mathbf{x}^T \mathbf{P}\mathbf{B}$ and $\mathbf{Q} \in \mathbb{R}^{2 \times 2}$ is positive definite and symmetric. Choose \mathbf{v} that renders \dot{V} negative, $\mathbf{v} = -\eta(\mathbf{x}) \frac{\omega}{\|\omega\|_2}$, where $\eta(\mathbf{x}) \geq \rho(\mathbf{x})$, so that

$$\begin{aligned}\dot{V} &= -\lambda_{\min}(\mathbf{Q})\|\mathbf{x}\|_2^2 - \frac{\omega^T \omega}{\|\omega\|_2} \eta(\mathbf{x}) + \|\omega\|_2 \rho(\mathbf{x}) \\ &= -\lambda_{\min}(\mathbf{Q})\|\mathbf{x}\|_2^2 + \|\omega\|_2 (\rho(\mathbf{x}) - \eta(\mathbf{x})) < 0 \quad \forall \mathbf{x} \in \mathbb{R}^4 \neq 0\end{aligned}$$

The redesign of \mathbf{v} stabilizes the system with uncertainties. Since \mathbf{v} is not smooth at the origin, we replace \mathbf{v} by the following smoothed version (see [2]):

$$\mathbf{v} = \begin{cases} -\eta(\mathbf{x}) \frac{\omega}{\|\omega\|_2} & \text{if } \eta(\mathbf{x}) \|\omega\|_2 \geq \gamma \\ -\eta(\mathbf{x}) \frac{\omega}{\gamma} & \text{if } \eta(\mathbf{x}) \|\omega\|_2 < \gamma \end{cases}$$

where $\gamma > 0$. The resulting closed-loop trajectories converge to a neighborhood of order γ about the origin. Since γ can be made arbitrarily small, the asymptotic set-point regulation error can be made negligible. This completes the robust nonlinear control design. Simulation results of the robust controller are shown in the next section.

IV. SIMULATION RESULTS

The closed-loop response of the nominal system using the ideal controller is shown in Figure 5. The maximum current attained with the given initial condition is 3.56 Amps. Small control inputs are achieved with this controller because of its large settling time.

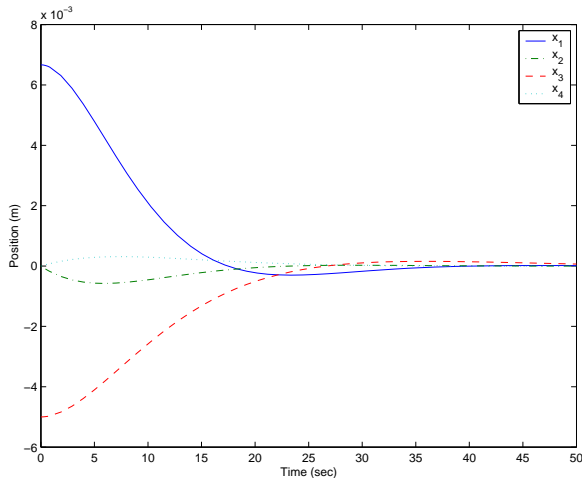


Fig. 5. Position and speed trajectories when using the ideal controller in the nominal system.

Figure 6 depicts the x and y positions of the ideal nonlinear controller and the robust nonlinear controller when applied to the system with the following uncertainties added: $\delta_1(x_1, x_2, x_3) \leq 1.1|x_1| + 1.1|x_3| - 0.01x_2$ and $\delta_2(x_1, x_3, x_4) \leq 1.1|x_1| + 1.1|x_3| - 0.01x_4$. The maximum of both upper bounds used by the robust controller is $\beta^* = 1.5$ low steady-state errors are achieved by setting $\gamma = 10^{-5}$. The ideal controller fails to stabilize the system while the robust controller manages to stabilize the system about the origin. Notice that although the robust redesign does not guarantee performance improvement, simulations suggest that transient response is improved with the robust controller.

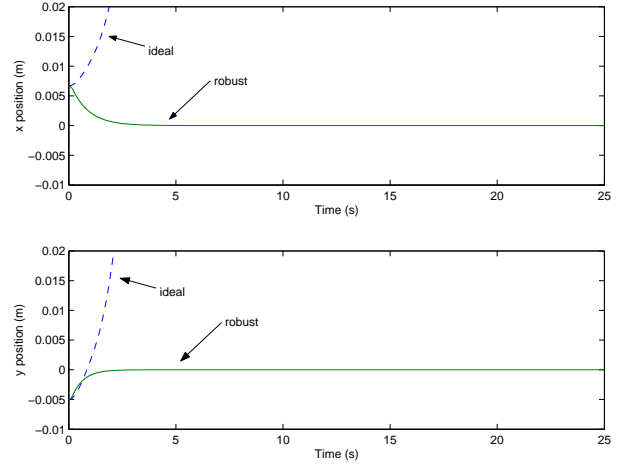


Fig. 6. Response of uncertain system when using ideal and robust nonlinear controllers.

Figure 7 shows the x and y positions of the robust nonlinear controller and an LQR controller designed from the linearized system. These two controllers were tested under the same condition as the last simulation. The linear controller is unable to stabilize the system with uncertainties while the robust nonlinear controller successfully stabilizes the system.

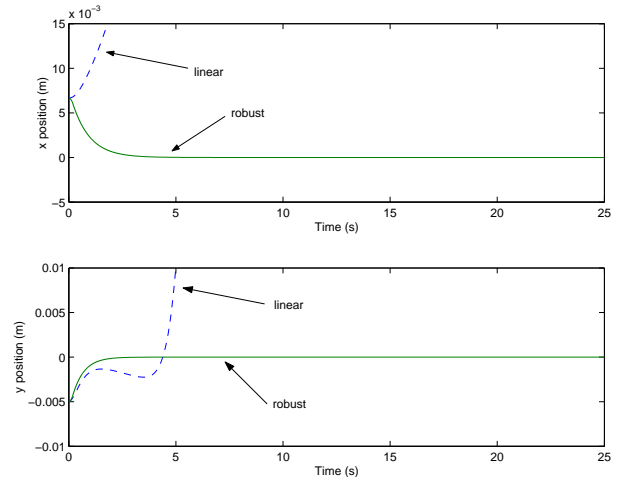


Fig. 7. Response of uncertain system when using a linear controller and the robust nonlinear controller.

The robust controller achieves a steady-state error of 9.4459×10^{-6} m at a maximum current of 3.7079 A. The currents of the robust controller are depicted in Figure 8. Although these results indicate that the robust controller can compensate for large uncertainties while maintaining high performance, there are some practical issues with using this controller, namely the chattering effect of the control inputs seen in Figure 8 that can excite high-frequency unmodelled dynamics in the system [4].

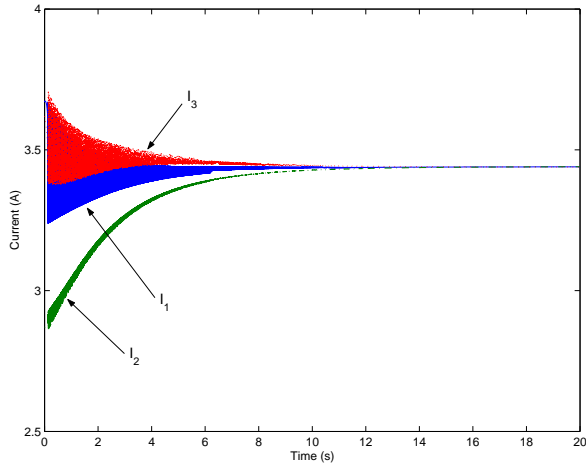


Fig. 8. Currents of robust nonlinear controller in uncertain system.

V. SUMMARY AND CONCLUSIONS

The modelling for a planar positioning device in a triangular arrangement has been derived and a robust nonlinear controller that handles a class of uncertainties has been designed. Although not significant in some cases, high control effort required by the robust redesign represents a drawback of this approach. Within an adaptive framework, friction and other uncertainties can be handled with smooth low currents. On the other hand, the ability of the robust controller to effectively reject uncertainties is desirable. Recently a robust adaptive controller was designed and found to perform well in the system. Large uncertainties are cancelled using robust methods while smaller uncertainties such as friction are compensated in a strict adaptive manner. Once the physical implementation of the planar magnetic device is complete, the robust controller and the robust adaptive controller will be tested on the actual system.

ACKNOWLEDGEMENTS

The authors would like to thank J.T. Spooner for providing inspiration for some of the ideas contained in this paper.

REFERENCES

- [1] Kenneth D. Demarest, *Engineering electromagnetics*, Prentice Hall, New Jersey, 1998.
- [2] Hassan K. Khalil, *Nonlinear systems*, second ed., Prentice Hall, Upper Saddle River, NJ 07458, 1995.
- [3] Ximin Shan, Shih-Kang Kuo, Jihua Zhang, , and Chia-Hsiang Menq, *Ultra precision motion control of a multiple degrees of freedom magnetic suspension stage*, IEEE/ASME Transactions on Mechatronics 7 (2002), 67–78.
- [4] Jean-Jackques E. Slotline and Weiping Li, *Applied nonlinear control*, first ed., Prentice Hall, Englewood Cliffs, NJ 07632, 1991.
- [5] J.T. Spooner, M. Maggiore, R. Ordóñez, and K.M. Passino, *Stable adaptive control and estimation for nonlinear systems: Neural and fuzzy approximator techniques*, John Wiley & Sons, New York, 2002.
- [6] David L. Trumper, *Modeling and vector control of planar magnetic levitator*, IEEE Transactions on Industry Applications 34 (1998), 1254–1262.
- [7] Herbert H. Woodson and James R. Melcher, *Electromechanical dynamics*, John Wiley & Sons, Inc., New York, 1968.